INVENTORY OF SUPPLEMENTAL MATERIAL

Supplemental Figures:

Supplemental Figure 1. Actin assembly properties of Cdc12 and For3 forced tandem FH2 domains.
Supplemental Figure 2. The fission yeast formins shift the critical concentration for actin assembly in the absence of profilin.
Supplemental Figure 3. Visualization of formin-mediated actin assembly by TIRF microscopy reveals differences in barbed end elongation rates.
Supplemental Figure 4. Both the For3 FH1 and FH2 domains may select against pyrene-labeled actin in the presence of profilin.
Supplemental Figure 5. Visualization of formin-mediated profilin-actin assembly by TIRF microscopy reveals differences in barbed end elongation rates.
Supplemental Figure 6. Protein sequence and predicted secondary structure alignment of FH2 domains from mouse mDia1, human DAAM1, worm CYK-1, budding yeast Bni1 and fission yeast Cdc12, Fus1 and For3.
Supplemental Figure 7. Mutations of conserved residues in the cytokinesis formin Cdc12 FH2 domain impair activity *in vitro* and *in vivo*.
Supplemental Figure 8. Mutations of conserved residues in the mating formin Fus1 FH2 domain impair activity *in vitro* and *in vivo*.
Supplemental Figure 9. Mutations of conserved residues in the polarity formin For3 FH2 domain impair activity *in vitro* and *in vivo*.
Supplemental Figure 10. Comparison of the actin assembly properties of the fission yeast formins before and after gel filtration.

Supplemental Videos:

Video 1. Related to Figure 2G and Supplemental Figure 3A-C. TIRF microscopy visualization of the assembly of 1.5 μM Mg-ATP-actin only.
Video 2. Related to Figure 2H and Supplemental Figure 3D-E. TIRF microscopy visualization of the assembly of 1.5 μM Mg-ATP-actin with 1 nM Cdc12(FH1FH2).
Video 3. Related to Figure 2I and Supplemental Figure 3G-I. TIRF microscopy visualization of the assembly of 1.5 μM Mg-ATP-actin with 0.5 nM Fus1(FH1FH2).
Video 4. Related to Figure 2J and Supplemental Figure 3J-L. TIRF microscopy visualization of the assembly of 1.5 μM Mg-ATP-actin with 150 nM For3(FH1FH2).
Video 5. Related to Figure 2K and Supplemental Figure 3M-O. TIRF microscopy visualization of the assembly of 1.5 μM Mg-ATP-actin with 50 nM For3(FH2).
Video 6. Related to Supplemental Figure 3P-R. TIRF microscopy visualization of the assembly of 1.5 μM Mg-ATP-actin with 500 nM For3(FH2).
Video 7. Related to Figure 3G and Supplemental Figure 5A-C. TIRF microscopy visualization of the assembly of 1.0 μM Mg-ATP-actin with 2.5 μM profilin.
Video 8. Related to Figure 3H and Supplemental Figure 5D-F. TIRF microscopy visualization of the assembly of 1.0 μM Mg-ATP-actin with 2.5 μM profilin and 2.5 nM Cdc12(FH1FH2).
Video 9. Related to Figure 3I and Supplemental Figure 5G-I. TIRF microscopy visualization of the assembly of 1.0 μM Mg-ATP-actin with 2.5 μM profilin and 5.0 nM Fus1(FH1FH2).
Video 10. Related to Figure 3J and Supplemental Figure 5J-L. TIRF microscopy visualization of the assembly of 1.0 μM Mg-ATP-actin with 2.5 μM profilin and 150 nM For3(FH1FH2).

SUPPLEMENTAL FIGURES

SUPPLEMENTAL FIGURE 1

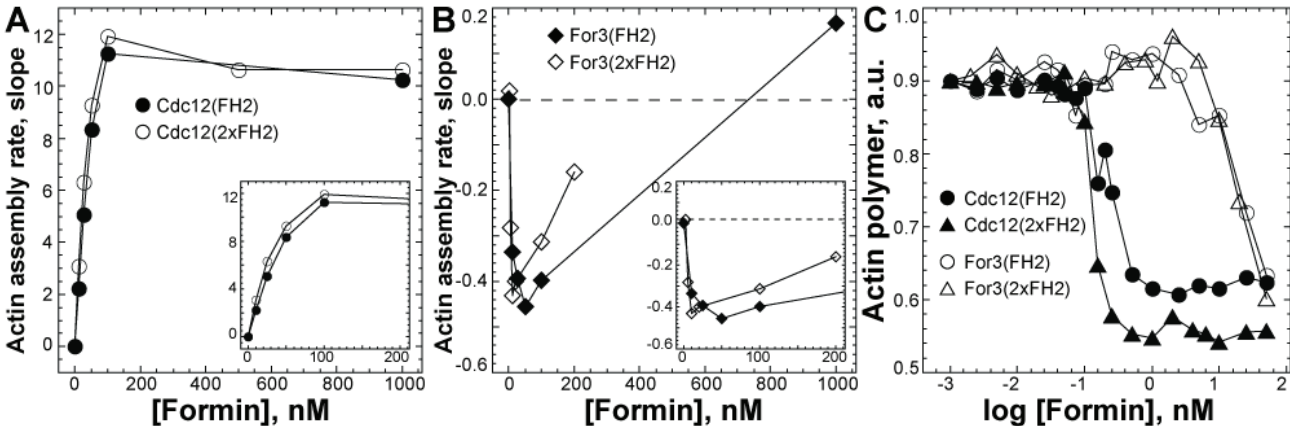

Supplemental Figure 1. Actin assembly properties of Cdc12 and For3 forced tandem FH2 domains. (A-B) Spontaneous actin assembly of 20% pyrene-labeled 2.5 μM Mg-ATP actin. Dependence of the actin assembly rate on formin concentration. Insets show plots with a focused x-axis. (A) Cdc12(FH2) (●), and MBP-Cdc12(FH2)::Cdc12(FH2) (○). (B) For3(FH2) (◆), and MBP-For3(FH2)::For3(FH2) (◇). (C) Critical concentration; dependence of polymer assembled from 1.0 μM actin (20% pyrene labeled) for 16 h on the concentration of Cdc12(FH2) (●), MBP-Cdc12(FH2)::Cdc12(FH2) (▲), For3(FH2) (○), and MBP-For3(FH2)::For3(FH2) (△).

SUPPLEMENTAL FIGURE 2

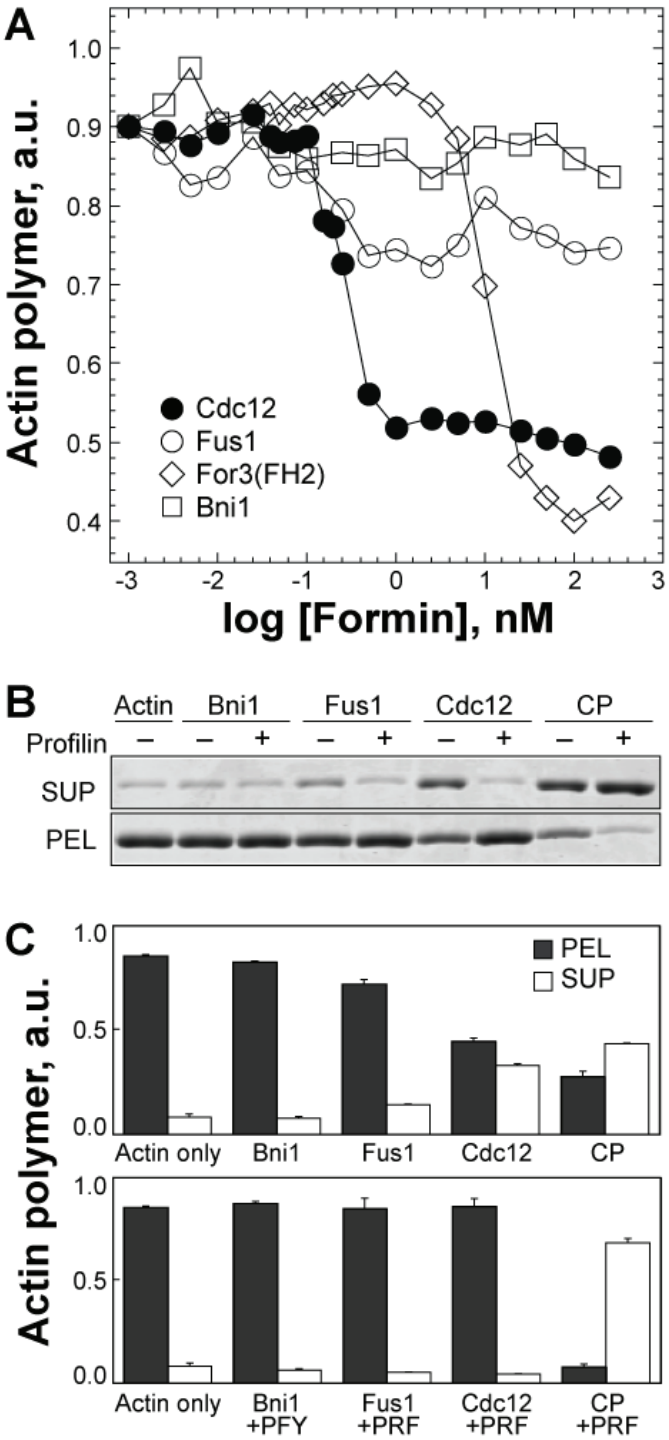

Supplemental Figure 2. The fission yeast formins shift the critical concentration for actin assembly in the absence of profilin. Polymer concentration of 1.0 μM actin after 16 hr of assembly, determined by either pyrene fluorescence (A) or centrifugation at 100,000*g* (B-C). (A) Dependence of actin polymer on the concentration of Cdc12(FH1FH2) (●), Fus1(FH1FH2) (○), For3(FH2) (◇), and Bni1(FH1FH2) (□). (B-C) Dependence of actin polymer on formin or mouse capping protein (CP) in either the absence or presence of 1.0 μM fission yeast profilin (PRF). (B) Representative Coomassie blue-stained gels showing actin in the supernatant (SUP) and pellet (PEL). (C) Bar graph of the average amount of actin in pellets (PEL) and supernatants (SUP). Error bars indicate standard deviation from three independent experiments.

SUPPLEMENTAL FIGURE 3

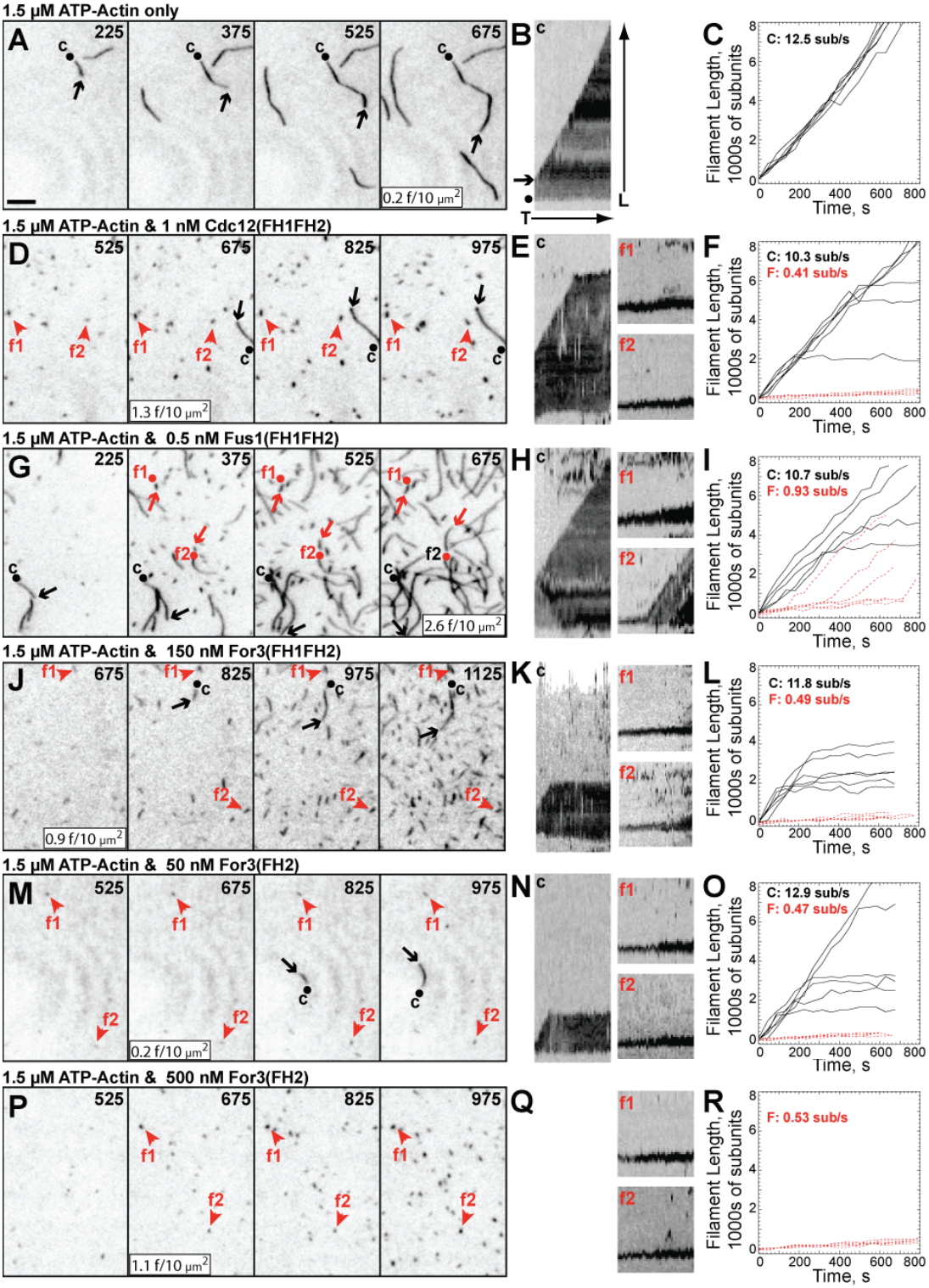

Supplemental Figure 3. Visualization of formin-mediated actin assembly by TIRF microscopy reveals differences in barbed end elongation rates. Spontaneous assembly of unlabeled 1.0 μM Mg-ATP-actin with 0.5 μM Mg-ATP-actin labeled with Oregon green. Scale bar = 5 μm. (A, D, G, J, M, P) Time-lapse micrographs with time in seconds indicated at the top. Arrows and dots indicate barbed and pointed ends. Arrowheads indicate formin-associated filaments too short to classify ends. Control filaments (c) and formin-associated filaments (f) are labeled in black and red. The average density of filaments in the entire field at 675 sec is indicated as filaments per 10 μm^2. (B, E, H, K, N, Q) Kymographs of the length (y axis) over time (x axis, 600s) of the filaments marked in time-lapse images. (C, F, I, L, O, R) The length of six individual filaments over time for control (solid lines) and formin-nucleated (red dashed lines) filaments. The average elongation rates are indicated (subunits/s). (A-C) Actin only control (Video 1). (D-F) 1.0 nM Cdc12(FH1FH2) (Video 2). (G-I) 0.5 nM Fus1(FH1FH2) (Video 3). (J-L) 150 nM For3(FH1FH2) (Video 4). (M-O) 50 nM For3(FH2) (Video 5). (P-R) 500 nM For3(FH2) (Video 6).

SUPPLEMENTAL FIGURE 4

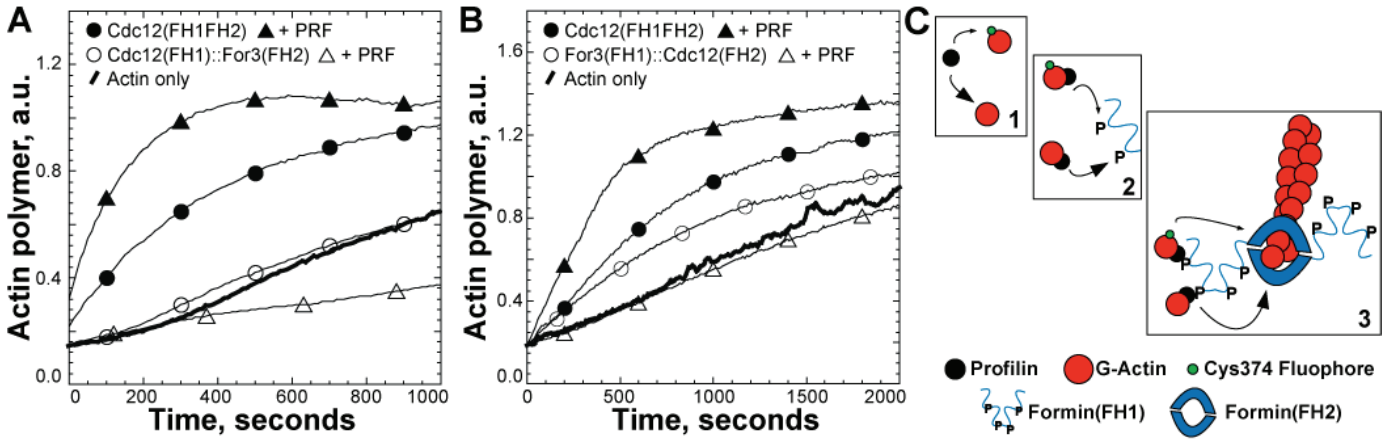

Supplemental Figure 4. Both the For3 FH1 and FH2 domains may select against pyrene-labeled actin in the presence of profilin. (A-B) Spontaneous assembly of 2.5 μM Mg-ATP actin monomers (20% pyrene-labeled) in the presence of chimeras mixing the FH1 and FH2 domains of Cdc12 and For3. (A) Time-course of pyrene fluorescence in the absence (thick curve) or presence of 10 nM Cdc12(FH1FH2) alone (●) and with 2.5 μM fission yeast profilin PRF (▲), or 750 nM $FH1^{cdc12}FH2^{For3}$ alone (○) and with PRF (△). (B) Time-course of pyrene fluorescence in the absence (thick curve) or presence of 10 nM Cdc12(FH1FH2) alone (●) and with 2.5 μM fission yeast profilin PRF (▲), or 500 nM $FH1^{For3}FH2^{Cdc12}$ alone (○) and with PRF (●). (C) Schematic of three steps in formin-mediated assembly of profilin-actin where selection against Cys374-labeled actin appears to occur: association of profilin with actin (1), association of profilin-actin with the FH1 domain (2), association of FH1-profilin-actin with the FH2-associated barbed end (3).

SUPPLEMENTAL FIGURE 5

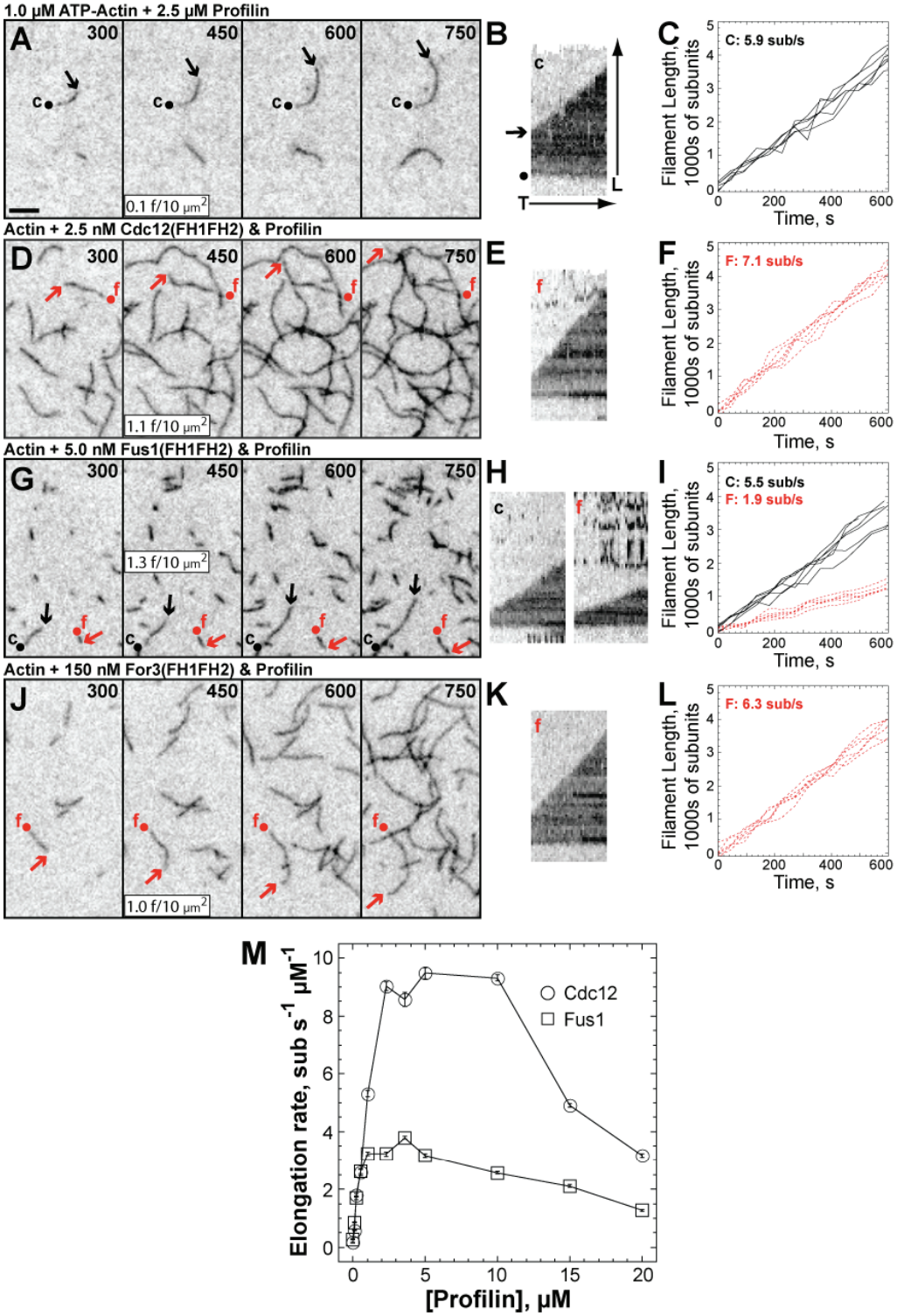

Supplemental Figure 5. Visualization of formin-mediated profilin-actin assembly by TIRF microscopy reveals differences in barbed end elongation rates. Spontaneous assembly of unlabeled 0.9 μM Mg-ATP-actin with 0.1 μM Mg-ATP-actin labeled on lysines with Alexa Green and 2.5 μM fission yeast profilin. (A, D, G, J) Time-lapse micrographs with time in seconds indicated at the top. Arrows and dots indicate barbed and pointed ends. Control filaments (c) and formin-associated filaments (f) are labeled in black and red. The average density of filaments in the entire field at 450 sec is indicated as filaments per 10 μm^2. Scale bar = 5 μm. (B, E, H, K) Kymographs of the length (y axis) over time (x axis, 600s) of the filaments marked in time-lapse images. (C, F, I, L) Length of six individual filaments versus time for control (solid lines) and/or formin-nucleated (red dashed lines) filaments. The average elongation rates are indicated (subunits/s). For Cdc12 and For3, control and formin-associated filaments could not be differentiated because they elongate at similar rates. (A-C) Actin and profilin control (Video 7). (D-F) 2.5 nM Cdc12(FH1FH2) and profilin (Video 8). (G-I) 5.0 nM Fus1(FH1FH2) and profilin (Video 9). (J-L) 150 nM For3(FH1FH2) and profilin (Video 10). (M) Dependence of the formin-associated filament elongation rate of 1.5 μM actin (0.5 μM Oregon green-labeled) on the concentration of profilin for 2.5 nM Cdc12(FH1FH2) (○) or Fus1(FH1FH2) (□).

SUPPLEMENTAL FIGURE 6

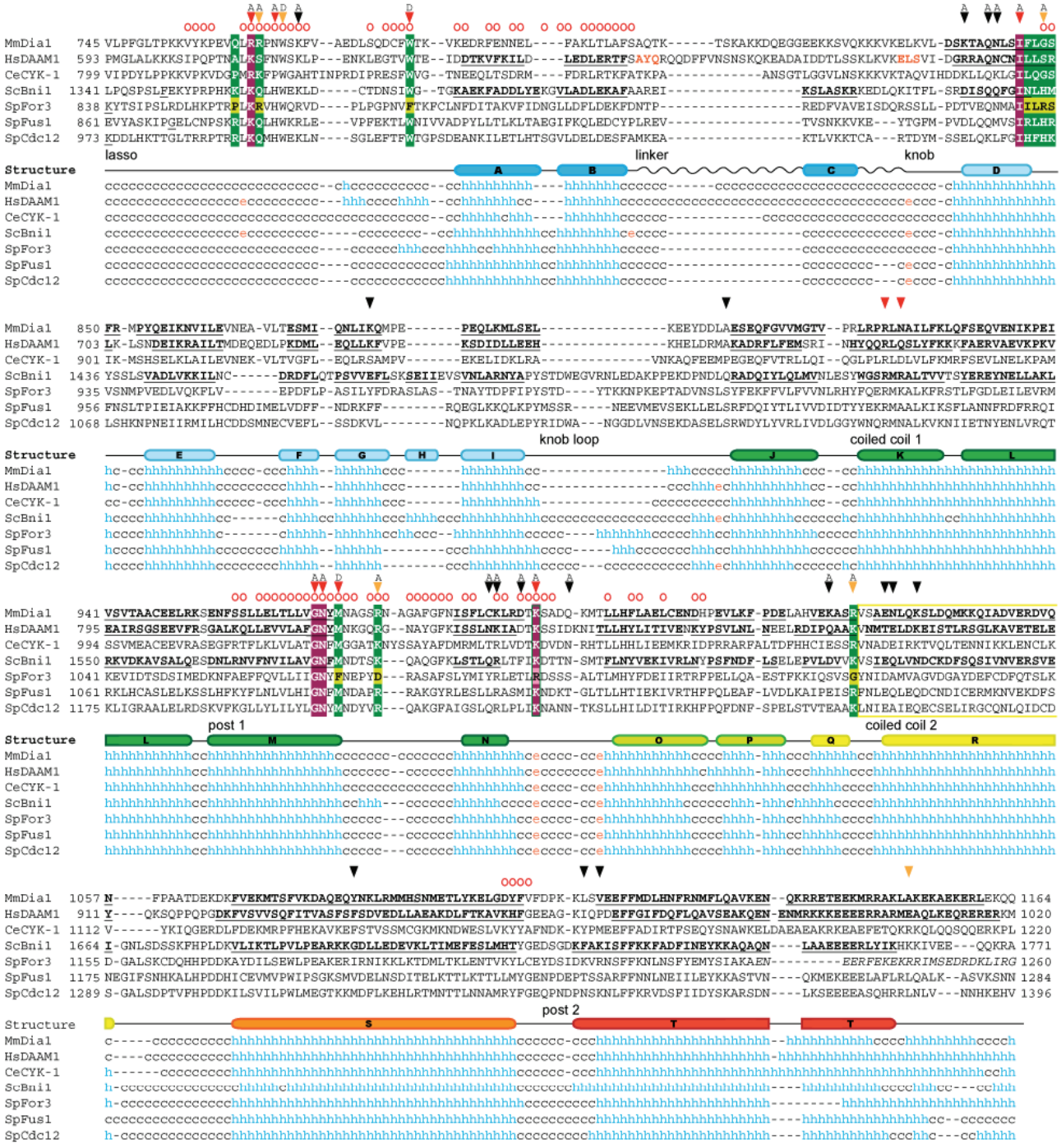

Supplemental Figure 6. Protein sequence and predicted secondary structure alignment of FH2 domains from mouse Dia1, human DAAM1, worm CYK-1, budding yeast Bni1 and fission yeast Cdc12, Fus1 and For3. Amino acid residues are indicated to the left of each line and at the end. Secondary structure elements are based on Bni1, mDia1 and DAAMI crystal structures (pdb 1ux5, 1v9d, 2j1d and 2z6e) (Shimada *et al.*, 2004; Xu *et al.*, 2004; Lu *et al.*, 2007; Yamashita *et al.*, 2007). Helices of Bni1, mDia1 and DAAM1 are underlined in the primary sequence, and are shown below the primary sequence as ovals in a rainbow color scheme (blue to red). Helices fold into a structure with four sub-regions from the N- to C-terminus: lasso, knob, coiled-coil, and post. Thin black lines below the primary sequence represent nonhelical regions. A wavy line indicates the linker connecting the lasso and knob. Predicted non-helical (black c) and helix (blue h) regions are aligned for each formin below the primary sequence. Above the primary sequence, red circles indicate residues in the lasso/post dimer interface. Triangles above the primary sequence indicate mutations characterized in this and previous studies (Sagot *et al.*, 2002; Xu *et al.*, 2004; Otomo *et al.*, 2005; Martin *et al.*, 2007; Yonetani and Chang, 2010), and letters denote sites predicted to be involved in actin binding (A) or dimerization (D). Triangle colors indicate severity of mutations on inhibiting actin assembly: red = high; orange = moderate; black = no effect. Shading of the primary sequence denotes positions we mutated in all fission yeast FH2 domains (purple), or mutated only in the For3 FH2 domain (green).

SUPPLEMENTAL FIGURE 7

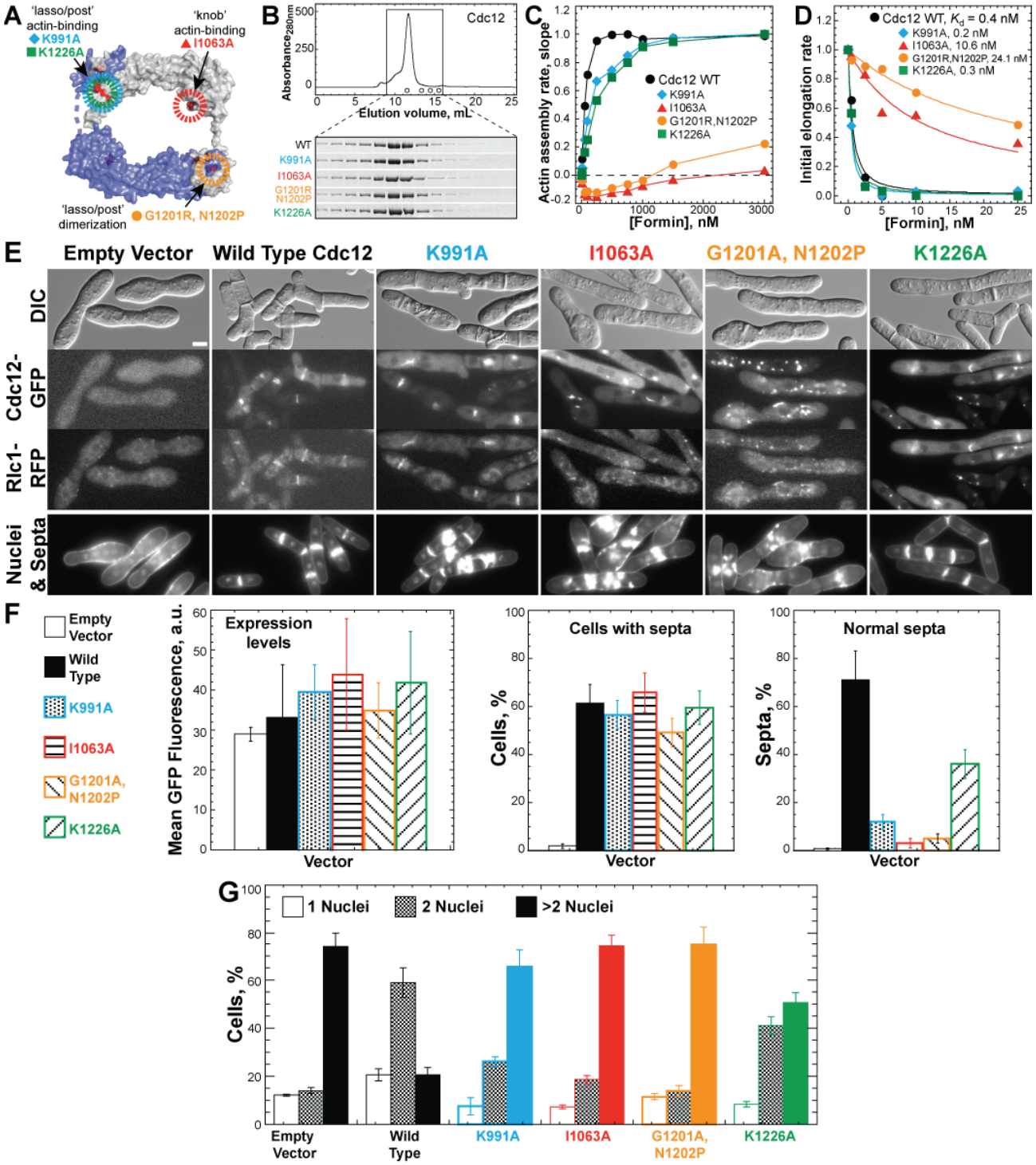

Supplemental Figure 7. Mutations of conserved residues in the cytokinesis formin Cdc12 FH2 domain impair activity *in vitro* and *in vivo*. (A) Location of Cdc12(FH2) amino acid mutations K991A (blue), I1063A (red), G1201R & N1202P (orange), and K1226A (green) indicated by circles on the FH2 dimer (monomers colored purple and gray), based on alignment with homologous residues in the budding yeast Bni1(FH2) structure (pdb 1y64) (Otomo *et al.*, 2005). (B) Gel filtration. Top: Profile of protein concentration over elution volume for wild type MBP-Cdc12(FH2). Peak elution volume of protein standards ferritin (440 kDa), aldolase (158 kDa), conalbumin (75 kDa), and ovalbumin (43 kDa) are indicated (○). Bottom: Coomassie Blue-stained gels of fractions spanning elution volumes 9-15 mL for the indicated MBP-Cdc12(FH2) constructs. (C) Spontaneous assembly of 20% pyrene-labeled 2.5 μM Mg-ATP actin monomers, as shown in Figure 6B. Dependence of the actin assembly rate (normalized slope) on the concentration of the indicated MBP-Cdc12(FH2) constructs. (D) Addition of 20% pyrene-labeled 0.2 μM Mg-ATP-actin monomer to 0.5 μM preassembled actin filament seeds. Dependence of barbed end elongation rate (normalized slope) on the concentration of the indicated MBP-Cdc12(FH2) constructs. Curve fits revealed the indicated equilibrium dissociation constants for the barbed end. (E-G) Morphology of the temperature sensitive mutant *cdc12-112* strain (KV427), expressing the indicated medium strength *p572-41X-cdc12(full-length)-GFP* constructs, following 16 hours at 36°C in EMM minimal media. (E) Representative micrographs of DIC, Cdc12-GFP and Rlc1-RFP (regulatory light chain) to visualize morphology and contractile rings, or stained with DAPI and calcofluor to visualize nuclei and septa. Scale bar = 5 μm. (F-G) Quantification of morphological features. Error bars specify standard deviation of triplicate experiments. (F) Expression level (left), percent of cells with septa (middle), and percent of septa that are normal (right), for the indicated constructs. (G) Percent of cells with 1, 2 or >2 nuclei for the indicated constructs. Part of this graph is also shown in Figure 6C.

SUPPLEMENTAL FIGURE 8

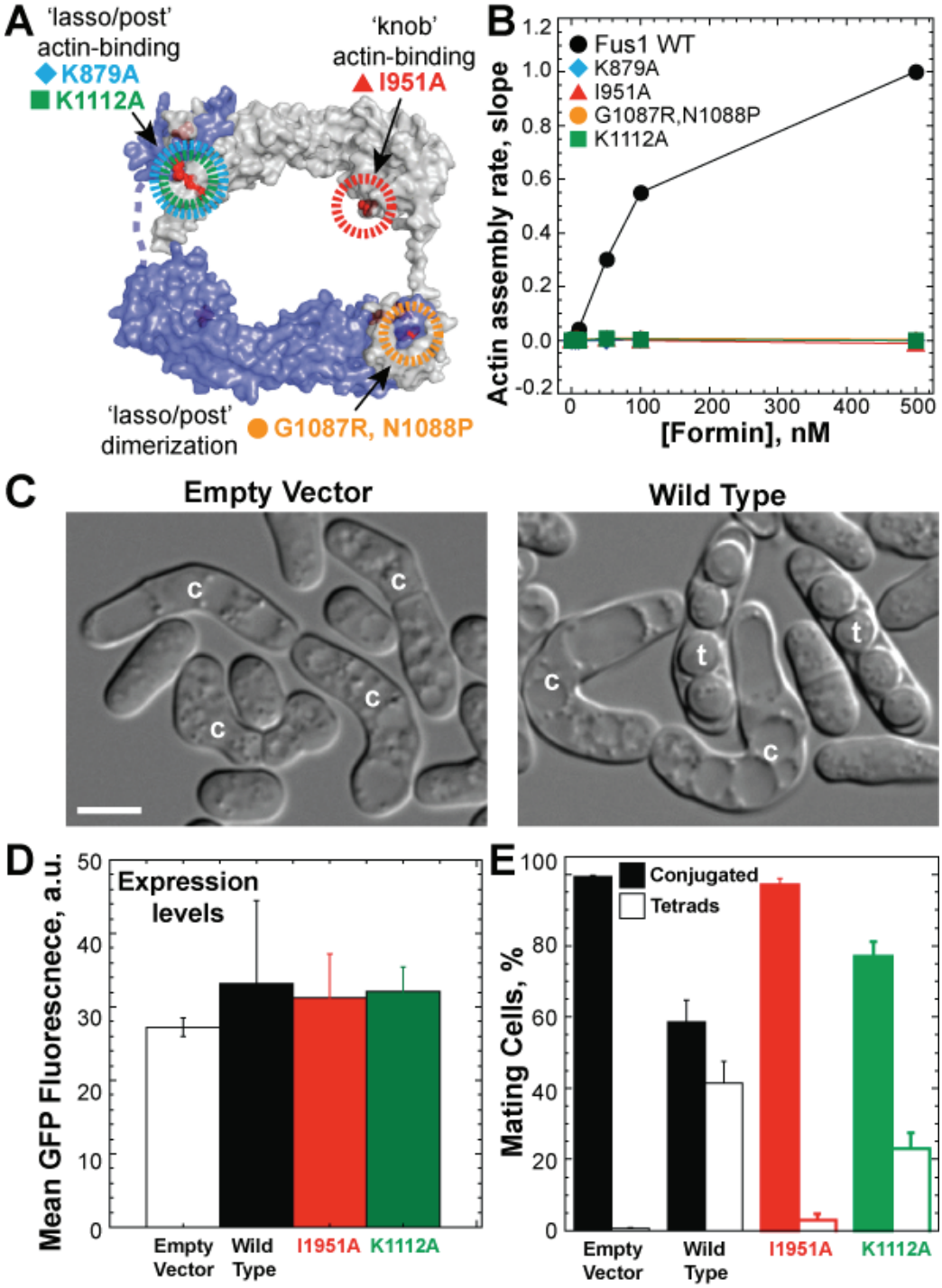

Supplemental Figure 8. Mutations of conserved residues in the mating formin Fus1 FH2 domain impair activity *in vitro* and *in vivo*. (A) Location of Fus1(FH2) amino acid mutations K879A (blue), I951A (red), G1087R & N1088P (orange), and K1112A (green) indicated by circles on the FH2 dimer (monomers colored purple and gray), based on alignment with homologous residues in the budding yeast Bni1(FH2) structure (pdb 1y64) (Otomo *et al.*, 2005). (B) Spontaneous assembly of 20% pyrene-labeled 2.5 μM Mg-ATP actin monomers, as shown in Figure 6D. Dependence of the actin assembly rate (normalized slope) on the concentration of the indicated MBP-Fus1(FH2) constructs. (C-E) Ability of h^{90} *fus1Δ* mutant cells (EG999; Petersen *et al.*, 1998) to mate and form tetrads following 36 hours at 25°C in ME media, upon expression of the indicated medium strength *p572-41X-fus1(full-length)-GFP* constructs. (C) Representative DIC micrographs demonstrating conjugated cells that have not formed tetrads (c), and conjugated cells that have formed tetrads (t). Scale bar = 5 μm. (D) Expression levels of each construct, determined by the mean GFP fluorescence. Errors bars represent standard deviations. (E) Percentage of mated cells that have and have not (conjugated) formed tetrads for the indicated constructs, as also reported in Figure 6E. Error bars signify the standard deviation of triplicate experiments.

SUPPLEMENTAL FIGURE 9

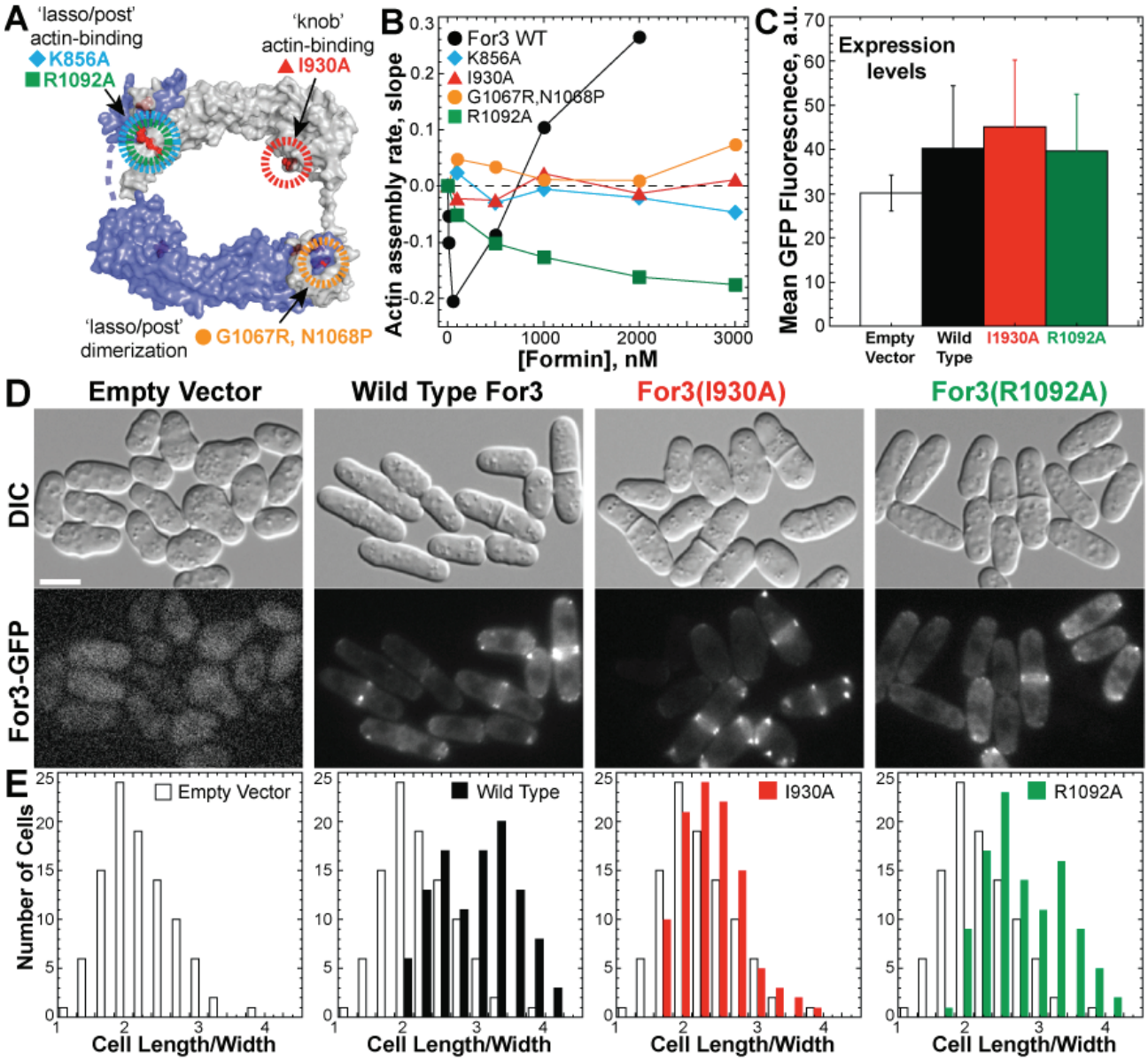

Supplemental Figure 9. Mutations of conserved residues in the polarity formin For3 FH2 domain impair activity *in vitro* and *in vivo*. (A) Location of For3(FH2) amino acid mutations K856A (blue), I930A (red), G1067R & N1068P (orange), and K1092A (green) indicated by circles on the FH2 dimer (monomers colored purple and gray), based on alignment with homologous residues in the budding yeast Bni1(FH2) structure (pdb 1y64) (Otomo *et al.*, 2005). (B) Spontaneous assembly of 20% pyrene-labeled 2.5 μM Mg-ATP actin monomers. Dependence of the actin assembly rate (slope) on the concentration of the indicated MBP-For3(FH2) constructs, as also reported in Figure 6F. (C-E) Morphology of *for3Δ* cells (strain BFY9; Feierbach and Chang, 2001), expressing medium strength *p572-41X-for3(full-length)-GFP* constructs, following 20 hours at 25°C in EMM minimal media. (C) Expression levels of each construct, determined by the mean GFP fluorescence. Errors bars represent standard deviations. (D) Representative DIC micrographs (morphology) and fluorescent GFP micrographs (localization of For3-GFP) of cells expressing the indicated constructs. Scale bar = 5 μm. (E) Histograms of the morphology (cell length/width) of at least 100 *for3Δ* cells expressing the indicated constructs. Empty vector cells are included in each histogram for comparison.

SUPPLEMENTAL FIGURE 10

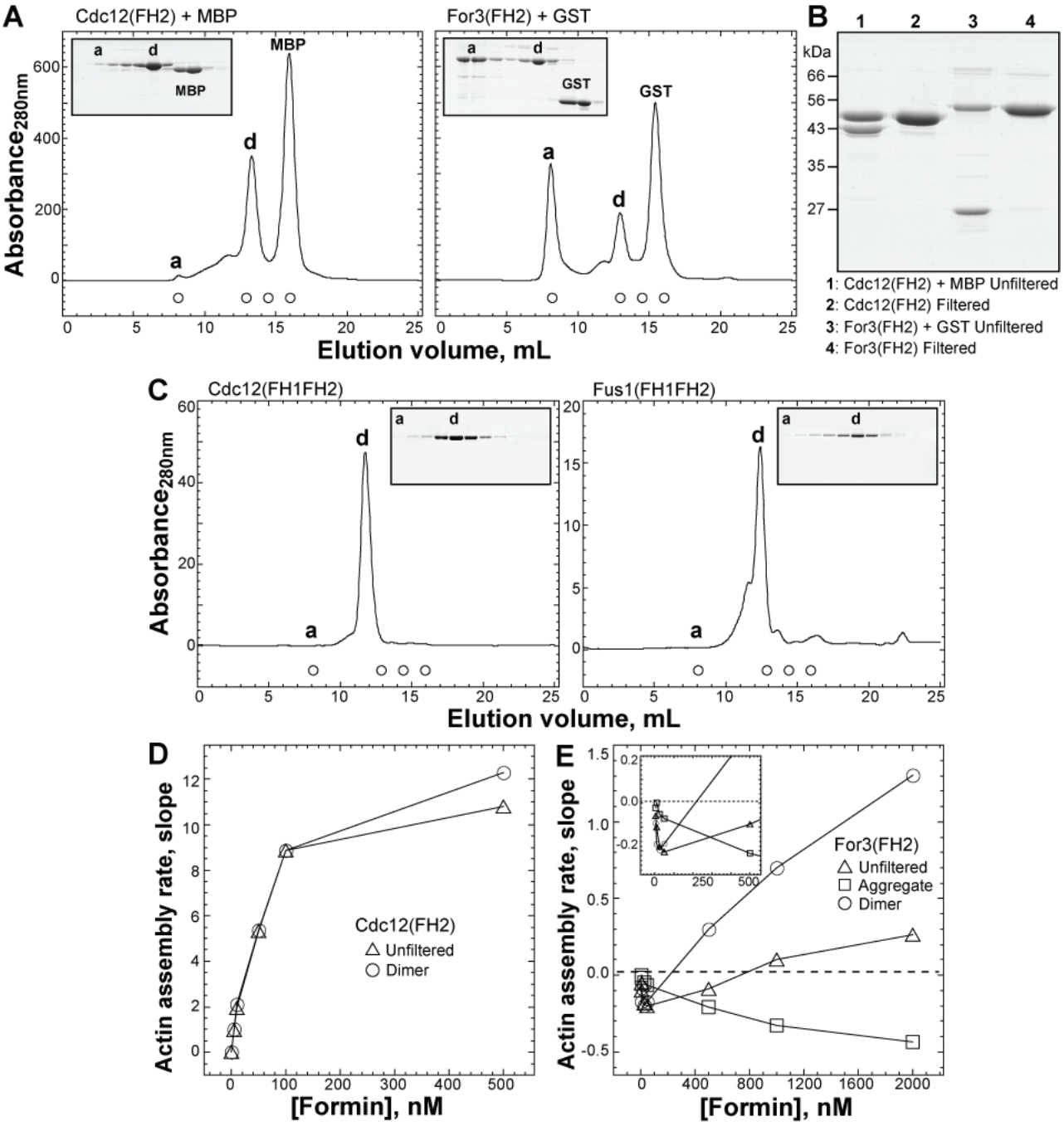

Supplemental Figure 10. Comparison of the actin assembly properties of the fission yeast formins before and after gel filtration. For3 forms stable active dimers, as well as higher order aggregates that do not stimulate actin assembly. (A-C) Gel filtration of Cdc12, For3 and Fus1. Proteins were flowed over a Superdex 200 10/300 gel filtration column. Peak elution volume of protein standards blue dextran (>2000 kDa), aldolase (158 kDa), conalbumin (75 kDa), and ovalbumin (43 kDa) are indicated (○). Peaks in elution profiles are designated as formin aggregates (a), formin dimers (d), GST or MBP. Insets show Coomassie-stained SDS-PAGE gels of elution volumes 7-17 mL. (A) MBP-Cdc12(FH2) and GST-For3(FH2) following 16 h of protease cleavage to remove the affinity tag. (B) Coomassie-stained SDS-PAGE gel of proteins before (Unfiltered) and after (Filtered) gel filtration. (C) Untagged Cdc12(FH1FH2) and Fus1(FH1FH2). (D-E) Spontaneous actin assembly of 20% pyrene-labeled 2.5 μM Mg-ATP-actin. (D) Dependence of the actin assembly rate on the concentration of unfiltered Cdc12(FH2) (△), and filtered Cdc12(FH2) dimer (○). (E) Dependence of the actin assembly rate on the concentration of unfiltered For3(FH2) (△), filtered For3(FH2) aggregate (□), and filtered For3(FH2) dimer (○). The inset shows the same plot with a focused x-axis.

SUPPLEMENTAL VIDEOS

Video 1. Related to Figure 2G and Supplemental Figure 3A-C. TIRF microscopy visualization of the assembly of 1.5 μM Mg-ATP-actin (33% Oregon green-labeled) only. 15 minutes played at 150X speed (6 sec). Wedges and dots indicate barbed and pointed ends. Control (c) filaments are labeled red.

Video 2. Related to Figure 2H and Supplemental Figure 3D-E. TIRF microscopy visualization of the assembly of 1.5 μM Mg-ATP-actin (33% Oregon green-labeled) with 1 nM Cdc12(FH1FH2). 15 minutes played at 150X speed (6 sec). Wedges and dots indicate barbed and pointed ends. Filled triangles indicate formin-associated filaments too short to classify ends. Control (c) and formin-associated (f) filaments are labeled red and blue.

Video 3. Related to Figure 2I and Supplemental Figure 3G-I. TIRF microscopy visualization of the assembly of 1.5 μM Mg-ATP-actin (33% Oregon green-labeled) with 0.5 nM Fus1(FH1FH2). 15 minutes played at 150X speed (6 sec). Wedges and dots indicate barbed and pointed ends. Control (c) and formin-associated (f) filaments are labeled red and blue.

Video 4. Related to Figure 2J and Supplemental Figure 3J-L. TIRF microscopy visualization of the assembly of 15 μM Mg-ATP-actin (33% Oregon green-labeled) with 150 nM For3(FH1FH2). 15 minutes played at 150X speed (6 sec). Wedges and dots indicate barbed and pointed ends. Filled triangles indicate formin-associated filaments too short to classify ends. Control (c) and formin-associated (f) filaments are labeled red and blue.

Video 5. Related to Figure 2K and Supplemental Figure 3M-O. TIRF microscopy visualization of the assembly of 1.5 μM Mg-ATP-actin (33% Oregon green-labeled) with 50 nM For3(FH2). 15 minutes played at 150X speed (6 sec). Wedges and dots indicate barbed and pointed ends. Filled triangles indicate formin-associated filaments too short to classify ends. Control (c) and formin-associated (f) filaments are labeled red and blue.

Video 6. Related to Supplemental Figure 3P-R. TIRF microscopy visualization of the assembly of 1.5 μM Mg-ATP-actin (33% Oregon green-labeled) with 500 nM For3(FH2). 15 minutes played at 150X speed (6 sec). Filled blue triangles indicate formin-associated filaments too short to classify ends.

Video 7. Related to Figure 3G and Supplemental Figure 5A-C. TIRF microscopy visualization of the assembly of 1.0 μM Mg-ATP-actin (10% Alexa green-labeled) with 2.5 μM profilin. 15 minutes played at 150X speed (6 sec). Wedges and dots indicate barbed and pointed ends. Control (c) filaments are labeled red.

Video 8. Related to Figure 3H and Supplemental Figure 5D-F. TIRF microscopy visualization of the assembly of 1.0 μM Mg-ATP-actin (10% Alexa green-labeled) with 2.5 μM profilin and 2.5 nM Cdc12(FH1FH2). 15 minutes played at 150X speed (6 sec). Wedges and dots indicate barbed and pointed ends. Putative formin-associated (f) filaments are labeled blue.

Video 9. Related to Figure 3I and Supplemental Figure 5G-I. TIRF microscopy visualization of the assembly of 1.0 μM Mg-ATP-actin (10% Alexa green-labeled) with 2.5 μM profilin and 5.0 nM Fus1(FH1FH2). 15 minutes played at 150X speed (6 sec). Wedges and dots indicate barbed and pointed ends. Control (c) and putative formin-associated (f) filaments are labeled red and blue.

Video 10. Related to Figure 3J and Supplemental Figure 5J-L. TIRF microscopy visualization of the assembly of 1.0 μM Mg-ATP-actin (10% Alexa green-labeled) with 2.5 μM profilin and 150 nM For3(FH1FH2). 15 minutes played at 150X speed (6 sec). Wedges and dots indicate barbed and pointed ends. Putative formin-associated (f) filaments are labeled blue.

SUPPLEMENTAL REFERENCES

Feierbach, B., and Chang, F. (2001). Roles of the fission yeast formin for3p in cell polarity, actin cable formation and symmetric cell division. Curr Biol *11*, 1656-1665.

Lu, J., Meng, W., Poy, F., Maiti, S., Goode, B.L., and Eck, M.J. (2007). Structure of the FH2 domain of Daam1: Implications for formin regulation of actin assembly. J Mol Biol *369*, 1258-1269.

Martin, S.G., Rincon, S.A., Basu, R., Perez, P., and Chang, F. (2007). Regulation of the formin for3p by cdc42p and bud6p. Mol Biol Cell *18*, 4155-4167.

Otomo, T., Tomchick, D.R., Otomo, C., Panchal, S.C., Machius, M., and Rosen, M.K. (2005). Structural basis of actin filament nucleation and processive capping by a formin homology 2 domain. Nature *433*, 488-494.

Petersen, J., Nielsen, O., Egel, R., and Hagan, I.M. (1998). FH3, a domain found in formins, targets the fission yeast formin Fus1 to the projection tip during conjugation. J Cell Biol *141*, 1217-1228.

Sagot, I., Rodal, A.A., Moseley, J., Goode, B.L., and Pellman, D. (2002). An actin nucleation mechanism mediated by Bni1 and profilin. Nat Cell Biol *4*, 626-631.

Shimada, A., Nyitrai, M., Vetter, I.R., Kuhlmann, D., Bugyi, B., Narumiya, S., Geeves, M.A., and Wittinghofer, A. (2004). The Core FH2 Domain of Diaphanous-Related Formins Is an Elongated Actin Binding Protein that Inhibits Polymerization. Mol Cell *13*, 511-522.

Xu, Y., Moseley, J.B., Sagot, I., Poy, F., Pellman, D., Goode, B.L., and Eck, M.J. (2004). Crystal structures of a formin homology-2 domain reveal a tethered dimer architecture. Cell *116*, 711-723.

Yamashita, M., Higashi, T., Suetsugu, S., Sato, Y., Ikeda, T., Shirakawa, R., Kita, T., Takenawa, T., Horiuchi, H., Fukai, S., and Nureki, O. (2007). Crystal structure of human DAAM1 formin homology 2 domain. Genes Cells *12*, 1255-1265.

Yonetani, A., and Chang, F. (2010). Regulation of cytokinesis by the formin cdc12p. Curr Biol *20*, 561-566.